Monthly Notices
of the
ROYAL ASTRONOMICAL SOCIETY

MNRAS **460,** L99–L103 (2016)
Advance Access publication 2016 April 29

doi:10.1093/mnrasl/slw084

An unexpected drop in the magnetic field of the X-ray pulsar V0332+53 after the bright outburst occurred in 2015

G. Cusumano,[1]★ V. La Parola,[1] A. D'Aì,[1] A. Segreto,[1] G. Tagliaferri,[2] S. D. Barthelmy[3] and N. Gehrels[3]

[1]*INAF - Istituto di Astrofisica Spaziale e Fisica Cosmica, Via U. La Malfa 153, I-90146 Palermo, Italy*
[2]*INAF - Brera Astronomical Observatory, via Bianchi 46, I-23807 Merate (LC), Italy*
[3]*NASA/Goddard Space Flight Center, Greenbelt, MD 20771, USA*

Accepted 2016 April 26. Received 2016 April 26; in original form 2016 January 29

ABSTRACT

How the accreted mass settling on the surface of a neutron star affects the topology of the magnetic field and how the secular evolution of the binary system depends on the magnetic field change is still an open issue. We report evidence for a clear drop in the observed magnetic field in the accreting pulsar V0332+53 after undergoing a bright 3-month long X-ray outburst. We determine the field from the position of the fundamental cyclotron line in its X-ray spectrum and relate it to the luminosity. For equal levels of luminosity, in the declining phase we measure a systematically lower value of the cyclotron line energy with respect to the rising phase. This results in a drop of $\sim 1.7 \times 10^{11}$ G of the observed field between the onset and the end of the outburst. The settling of the accreted plasma on to the polar cap seems to induce a distortion of the magnetic field lines weakening their intensity along the accretion columns. Therefore, the dissipation rate of the magnetic field could be much faster than previously estimated, unless the field is able to restore its original configuration on a time-scale comparable with the outbursts recurrence time.

Key words: magnetic fields – pulsars: individual: V0332+53 – X-rays: binaries.

1 INTRODUCTION

Neutron stars (NS) in high-mass X-ray binaries are powered by the release of gravitational energy from the matter accreting from their companion star. The magnetic field of the NS ($\sim 10^{12}$ G) drives the accreting matter along its field lines towards the magnetic polar caps. As a result an accretion column forms, where matter is slowed up by radiative processes that produce X-rays.

The same magnetic field modifies the radiation emitted in the regions above the polar caps: in the presence of such a strong magnetic field, the kinetic energy of the electrons in the accreting plasma is quantized in discrete Landau levels and photons with energies corresponding to these levels undergo resonant scattering, imprinting on the X-ray spectrum cyclotron resonant scattering features (CRSF). The energy of the fundamental line provides a direct measure of the magnetic field in the region where the line is produced, according to the relation $E_{\rm cyc} = 11.68 \times B_{12}/(1 + z)$ keV, where z is the gravitational redshift in the line-forming region and B_{12} is the magnetic field in units of 10^{12} G. CRSFs have been observed in ∼20 pulsars (Revnitsev & Mereghetti 2015), probing magnetic fields in the range (0.1–5) $\times 10^{12}$ G. In some sources, it has been observed that the position of the line changes as a function of the luminosity implying that the optically thick region where the line is imprinted moves along the accretion columns for as much as some hundred metres (Becker et al. 2012).

V0332+53 is an accreting X-ray pulsar with a spin period of ∼4.4 s, orbiting around an early type companion star (Negueruela et al. 1999) in an eccentric orbit of ∼34 d (Stella et al. 1985). The source shows sporadic giant X-ray outbursts lasting several weeks, followed by years-long intervals of quiescence. In 1989, an outburst recorded by the Ginga observatory revealed the presence of a cyclotron absorption feature (Makishima et al. 1990) at ∼28.5 keV, corresponding to a magnetic field of $\sim 2.5 \times 10^{12}(1 + z)$ G. Between 2004 November and 2005 February, a giant outburst was monitored with the Rossi XTE and Integral observatories in the X-ray band (Mowlavi et al. 2006; Tsygankov et al. 2006; Tsygankov, Lutovinov & Serber 2010). The position of the peak energy of the cyclotron line changed during the outburst in anticorrelation with the luminosity, going from ∼30 keV at the onset of the outburst to ∼24 keV at the luminosity peak, and returning to ∼30 keV at the end of the outburst, following the same track in both the brightening and the fading phase. This is interpreted with the infalling plasma being decelerated along the accretion columns by a radiation dominated shock (Basko & Sunyaev 1976; Burnard, Arons & Klein 1991; Becker et al. 2012), whose height above the NS surface increases

★ E-mail: cusumano@ifc.inaf.it.

© 2016 The Authors
Published by Oxford University Press on behalf of the Royal Astronomical Society

Downloaded from https://academic.oup.com/mnrasl/article-abstract/460/1/L99/2589767 by guest on 23 April 2020

with luminosity. If the height of the line-forming region follows the height of the shock, the observed anticorrelation is straightforwardly explained as the magnetic field weakens with the distance from the polar cap.

This Letter is focused on the study of the CRSF evolution during the bright outburst of V0332+53 occurred in 2015. Section 2 describes the Burst Alert Telescope (BAT) and X-Ray Telescope (XRT) data reduction. Section 3 describes the broad-band spectral analysis. In Section 4, we discuss our results.

2 DATA REDUCTION

V0332+53 went into outburst between 2015 June and September. The BAT (Barthelmy et al. 2005) on board the Swift observatory (Gehrels et al. 2004) performed a nearly continuous monitoring in the 15–150 keV energy band, while the Swift XRT (Burrows et al. 2005) covered the soft X-ray band (0.6–10 keV) with several pointed observations. BAT is a coded mask telescope that observes the sky in the 15–150 keV energy range with a field of view of 1.4 steradian (half coded). It is devoted to an all-sky monitoring with the main aim of capturing gamma ray burst events. The pointing strategy of Swift, that performs frequent slews to observe different sky directions, allows BAT to monitor more than 80 per cent of the entire sky every day. V0332+53 was observed by BAT with a daily duty-cycle of ∼20 per cent. The BAT survey data stored in the HEASARC public archive[1] were processed with the BAT_IMAGER code (Segreto et al. 2010), a software built for the analysis of data from coded mask instruments that performs screening, mosaicking and source detection. The background subtracted light curve and spectra of V0332+53 were produced with the maximum time resolution allowed by the data (typically 300 s). To obtain spectra with similar and sufficient statistics, we selected time intervals of different duration to achieve a minimum signal-to-noise ratio (SNR) of 300. Only for the first and the last interval, in order to measure $E_{\rm cyc}$ at the lowest fluxes, the spectra were cumulated with a lower SNR (∼150). With this selection, we obtained 22 spectra. We used the official BAT spectral redistribution matrix.[2] XRT (0.2–10 keV) observed V0332+53 thirty-one times during the outburst. For each BAT spectral time interval, we used only the temporally closest XRT observation. All the selected observations are in Windowed Timing mode (Hill et al. 2004). The XRT data were processed with standard filtering and screening criteria (XRTPIPELINE v.0.12.4, HEASOFT v. 6.12). For each observation, we extracted the spectrum by selecting data from a rectangular region of 40 pixel side along the image strip (1 pixel = 2.36 arcsec) centred on the source brightest pixel; the background was extracted from a region of the same size far from the source extraction region. The spectra were re-binned with a minimum of 20 counts per energy channel to allow for the use of χ^2 statistics. The XRT ancillary response files were generated with XRTMKARF.[3] We used the spectral redistribution matrix v014; the spectral analysis was performed using XSPEC v.12.5. Errors are reported at 68 per cent confidence level. The luminosity of the source has been evaluated using the 1–150 keV flux derived from the best-fitting model of the continuum and assuming isotropic emission at a distance of 7 kpc (Negueruela et al. 1999).

[1] http://heasarc.gsfc.nasa.gov/docs/archive.html
[2] http://heasarc.gsfc.nasa.gov/docs/heasarc/caldb/data/swift/bat/index.html
[3] http://heasarc.gsfc.nasa.gov/ftools/caldb/help/xrtmkarf.html

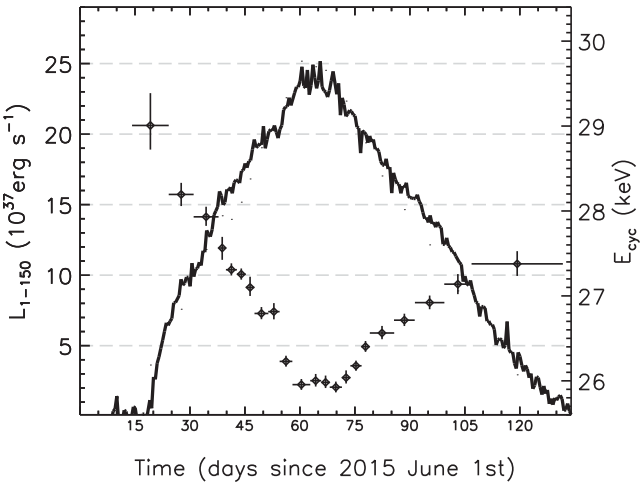


Figure 1. Temporal evolution of the X-ray luminosity (left axis, solid line) and of the energy of the CRSF fundamental line (right axis, diamond points) The horizontal error bars represent the time interval corresponding to each spectrum.

3 DATA ANALYSIS

Fig. 1 shows the 1–150 keV luminosity (L_{1-150}) of the 2015 outburst derived from the BAT monitoring. Its shape can be described with a linear rise and decline, roughly specular with respect to a peak that lasted ∼10 d reaching a luminosity of $\sim 2.5 \times 10^{38}$ erg s^{-1}.

To cope with the non-simultaneity of the BAT and XRT data, we included in the spectral model a multiplicative factor that takes into account any mismatch in intensity between the hard and soft data. To model the continuum emission of the source we tested different spectral shapes, modified at low energy by photoelectric absorption along the line of sight: a simple power law modified with an exponential cut-off, a negative–positive power laws with exponential cutoff (Mihara, Makishima & Nagase 1995), an optically thick Comptonization (`comptt` in XSPEC). We verified that the choice of the continuum model does not affect the results discussed in this Letter. In the following, we will adopt a continuum described by a power law modified with an exponential cut-off (`cutoffpl` in XSPEC). We included in the model two CRSFs, the fundamental line and its second harmonic, using absorption Gaussian profiles (`gabs` in XSPEC). The residuals in all the 22 spectra do not statistically require any additional component to model the fundamental CRSF. The results of the spectral analysis are reported in Table 1. The continuum emission does not show any noteworthy variability: the photon index does not change significantly along the outburst, while the cutoff energy ranges between 6.2 and 7.1 keV. The position of the fundamental (Fig. 1), the line width and its depth are determined on average with relative uncertainties of ∼0.3, 2.8, and 4.3 per cent, respectively. The relative uncertainties on the parameters of the second harmonic (detected at ∼50 keV) are much higher, and in the following we will focus only on the energy of the fundamental line ($E_{\rm cyc}$). Fig. 2 shows the data, best-fitting model and residuals for two representative spectra with similar luminosity in the rise and decline (spectra 2 and 21 in Table 1).

The cyclotron energy shows a clear anticorrelation with luminosity (Fig. 4, black diamonds). Moreover, the cyclotron energy describes clearly two different diverging tracks for the outburst rise and decline, being systematically lower after the peak, reaching a final value of 27.68 ± 0.15 keV versus an initial value of $29.2^{+0.4}_{-0.3}$ keV. We investigated the correlation between $E_{\rm cyc}$ and the other fit

Downloaded from https://academic.oup.com/mnrasl/article-abstract/460/1/L99/2589767 by guest on 23 April 2020

Table 1. Best-fitting spectral parameters for each BAT+XRT broad-band spectrum. The second column lists the central time of each spectrum in days, referred to MJD 57188.24 (the start time of the first spectrum) The broad-band X-ray model used to fit the continuum is a power law with photon index Γ and normalization $N_{\rm cpl}$ in photons kev^{-1}cm^{-2}s^{-1} at 1 keV, modified by an exponential cutoff at energy $E_{\rm cut}$ (keV). The model includes also photoelectric absorption by neutral interstellar matter ($N_{\rm H}$, in units of 10^{22} atoms cm^{-2}). The CRSFs are modelled with two Gaussians in absorption for the fundamental and the second harmonic, respectively. The central energies $E_{\rm cyc}$ and E_2 and the line widths $\sigma_{\rm cyc}$ and σ_2 are in keV. $D_{\rm cyc}$ and D_2 are the optical depths of the features. The luminosity in the 1–150 keV range is in units of 10^{37} erg s^{-1}.

	Time	$N_{\rm H}$	Γ	$E_{\rm cut}$	$N_{\rm cpl}$	$E_{\rm cyc}$	$\sigma_{\rm cyc}$	$D_{\rm cyc}$	E_2	σ_2	D_2	L_{1-150}	$\chi^2_{\rm red}$(dof)
1	5.00	$0.79^{+0.11}_{-0.10}$	$-0.08^{+0.09}_{-0.06}$	$6.7^{+0.7}_{-0.3}$	$0.07^{+0.01}_{-0.01}$	$29.2^{+0.4}_{-0.3}$	$3.6^{+0.4}_{-0.3}$	$1.2^{+0.3}_{-0.2}$	50^{+3}_{-2}	$3.8^{+2.2}_{-1.6}$	$1.3^{+1.4}_{-0.8}$	3.6	1.07(494)
2	13.38	$0.81^{+0.10}_{-0.09}$	$-0.06^{+0.04}_{-0.05}$	$6.91^{+0.14}_{-0.13}$	$0.15^{+0.01}_{-0.01}$	$28.39^{+0.14}_{-0.14}$	$3.77^{+0.14}_{-0.14}$	$1.25^{+0.08}_{-0.07}$	$48.9^{+1.0}_{-0.6}$	$3.6^{+0.9}_{-0.7}$	$0.9^{+0.4}_{-0.3}$	7.6	1.09(494)
3	20.18	$0.85^{+0.10}_{-0.10}$	$-0.03^{+0.05}_{-0.05}$	$7.12^{+0.20}_{-0.16}$	$0.23^{+0.02}_{-0.02}$	$28.13^{+0.12}_{-0.11}$	$4.08^{+0.13}_{-0.12}$	$1.32^{+0.09}_{-0.07}$	$48.6^{+0.9}_{-0.7}$	$3.4^{+0.8}_{-0.6}$	$1.6^{+0.6}_{-0.4}$	11.8	1.14(494)
4	24.58	$0.84^{+0.10}_{-0.10}$	$-0.03^{+0.06}_{-0.06}$	$7.10^{+0.41}_{-0.29}$	$0.28^{+0.02}_{-0.02}$	$27.76^{+0.13}_{-0.14}$	$4.19^{+0.17}_{-0.16}$	$1.31^{+0.13}_{-0.11}$	52^{+2}_{-2}	$5.9^{+1.4}_{-1.3}$	$1.6^{+0.9}_{-0.6}$	14.2	1.12(494)
5	27.05	$0.82^{+0.10}_{-0.10}$	$-0.05^{+0.05}_{-0.05}$	$6.92^{+0.14}_{-0.12}$	$0.28^{+0.02}_{-0.02}$	$27.51^{+0.08}_{-0.07}$	$3.81^{+0.10}_{-0.09}$	$1.23^{+0.06}_{-0.05}$	$48.6^{+0.6}_{-0.4}$	$3.5^{+0.6}_{-0.5}$	$1.3^{+0.3}_{-0.2}$	14.0	1.15(493)
6	29.75	$0.82^{+0.10}_{-0.10}$	$-0.05^{+0.05}_{-0.05}$	$6.95^{+0.13}_{-0.12}$	$0.30^{+0.02}_{-0.02}$	$27.46^{+0.07}_{-0.06}$	$3.81^{+0.09}_{-0.09}$	$1.28^{+0.05}_{-0.05}$	$49.3^{+0.6}_{-0.5}$	$3.6^{+0.5}_{-0.4}$	$1.6^{+0.3}_{-0.3}$	15.2	1.10(493)
7	32.17	$0.89^{+0.10}_{-0.10}$	$-0.04^{+0.05}_{-0.05}$	$6.87^{+0.11}_{-0.10}$	$0.35^{+0.03}_{-0.02}$	$27.20^{+0.06}_{-0.06}$	$3.81^{+0.08}_{-0.08}$	$1.29^{+0.05}_{-0.04}$	$48.7^{+0.5}_{-0.5}$	$3.9^{+0.5}_{-0.4}$	$1.3^{+0.2}_{-0.2}$	16.8	1.10(510)
8	35.23	$0.82^{+0.10}_{-0.10}$	$-0.07^{+0.05}_{-0.05}$	$6.66^{+0.12}_{-0.11}$	$0.39^{+0.03}_{-0.03}$	$26.99^{+0.08}_{-0.07}$	$4.10^{+0.09}_{-0.08}$	$1.26^{+0.05}_{-0.04}$	$49.5^{+0.8}_{-0.6}$	$3.9^{+0.7}_{-0.6}$	$1.3^{+0.3}_{-0.3}$	19.0	1.12(494)
9	38.68	$0.82^{+0.10}_{-0.10}$	$-0.07^{+0.06}_{-0.05}$	$6.78^{+0.23}_{-0.16}$	$0.40^{+0.03}_{-0.03}$	$27.01^{+0.10}_{-0.09}$	$4.21^{+0.12}_{-0.10}$	$1.32^{+0.09}_{-0.07}$	$49.5^{+0.7}_{-0.7}$	$4.8^{+0.9}_{-0.8}$	$1.2^{+0.4}_{-0.3}$	20.2	1.10(494)
10	41.97	$0.78^{+0.10}_{-0.10}$	$-0.11^{+0.05}_{-0.05}$	$6.42^{+0.11}_{-0.10}$	$0.45^{+0.04}_{-0.03}$	$26.43^{+0.07}_{-0.06}$	$4.21^{+0.09}_{-0.08}$	$1.26^{+0.05}_{-0.04}$	$47.8^{+0.6}_{-0.5}$	$3.4^{+0.5}_{-0.4}$	$1.2^{+0.3}_{-0.2}$	22.6	1.13(494)
11	46.13	$0.76^{+0.10}_{-0.10}$	$-0.14^{+0.05}_{-0.05}$	$6.21^{+0.10}_{-0.09}$	$0.51^{+0.04}_{-0.04}$	$26.16^{+0.07}_{-0.06}$	$4.31^{+0.09}_{-0.08}$	$1.18^{+0.05}_{-0.04}$	$48.3^{+0.6}_{-0.6}$	$3.1^{+0.7}_{-0.5}$	$1.2^{+0.3}_{-0.3}$	25.2	1.15(494)
12	50.05	$0.75^{+0.10}_{-0.10}$	$-0.14^{+0.05}_{-0.05}$	$6.21^{+0.11}_{-0.10}$	$0.49^{+0.04}_{-0.04}$	$26.20^{+0.08}_{-0.07}$	$4.37^{+0.10}_{-0.09}$	$1.19^{+0.06}_{-0.05}$	$47.6^{+0.8}_{-0.6}$	$3.4^{+0.8}_{-0.6}$	$0.9^{+0.3}_{-0.2}$	24.8	1.16(494)
13	52.71	$0.75^{+0.10}_{-0.10}$	$-0.14^{+0.05}_{-0.05}$	$6.23^{+0.12}_{-0.10}$	$0.49^{+0.04}_{-0.04}$	$26.18^{+0.08}_{-0.07}$	$4.27^{+0.10}_{-0.09}$	$1.18^{+0.06}_{-0.04}$	$48.7^{+1.1}_{-0.9}$	$3.8^{+1.1}_{-0.8}$	$0.9^{+0.4}_{-0.3}$	24.5	1.15(494)
14	55.54	$0.75^{+0.10}_{-0.10}$	$-0.15^{+0.05}_{-0.05}$	$6.14^{+0.10}_{-0.10}$	$0.46^{+0.04}_{-0.03}$	$26.13^{+0.07}_{-0.06}$	$4.19^{+0.09}_{-0.08}$	$1.14^{+0.04}_{-0.04}$	$49.2^{+0.8}_{-0.7}$	$3.5^{+0.7}_{-0.6}$	$1.4^{+0.4}_{-0.3}$	23.1	1.14(494)
15	58.36	$0.75^{+0.10}_{-0.10}$	$-0.14^{+0.05}_{-0.05}$	$6.26^{+0.14}_{-0.11}$	$0.44^{+0.03}_{-0.03}$	$26.24^{+0.09}_{-0.07}$	$4.24^{+0.10}_{-0.09}$	$1.19^{+0.06}_{-0.05}$	51^{+2}_{-1}	$4.5^{+1.4}_{-0.9}$	$1.3^{+0.7}_{-0.4}$	22.3	1.11(494)
16	61.05	$0.75^{+0.10}_{-0.10}$	$-0.15^{+0.05}_{-0.05}$	$6.22^{+0.10}_{-0.10}$	$0.41^{+0.03}_{-0.03}$	$26.38^{+0.06}_{-0.06}$	$4.12^{+0.08}_{-0.07}$	$1.19^{+0.04}_{-0.04}$	$48.2^{+0.7}_{-0.6}$	$3.0^{+0.5}_{-0.5}$	$1.4^{+0.3}_{-0.3}$	20.6	1.15(494)
17	63.69	$0.77^{+0.10}_{-0.10}$	$-0.12^{+0.05}_{-0.05}$	$6.37^{+0.11}_{-0.10}$	$0.39^{+0.03}_{-0.03}$	$26.60^{+0.07}_{-0.06}$	$4.10^{+0.08}_{-0.07}$	$1.24^{+0.05}_{-0.04}$	$48.5^{+1.0}_{-0.8}$	$3.5^{+0.8}_{-0.6}$	$1.0^{+0.3}_{-0.2}$	19.4	1.12(494)
18	68.12	$0.79^{+0.10}_{-0.10}$	$-0.10^{+0.05}_{-0.05}$	$6.56^{+0.17}_{-0.13}$	$0.34^{+0.03}_{-0.02}$	$26.76^{+0.08}_{-0.07}$	$3.99^{+0.10}_{-0.08}$	$1.29^{+0.07}_{-0.05}$	$49.5^{+1.0}_{-0.8}$	$4.7^{+0.9}_{-0.7}$	$1.3^{+0.4}_{-0.3}$	17.0	1.14(494)
19	74.28	$0.81^{+0.10}_{-0.10}$	$-0.07^{+0.05}_{-0.05}$	$6.71^{+0.16}_{-0.13}$	$0.29^{+0.02}_{-0.02}$	$26.91^{+0.08}_{-0.07}$	$3.92^{+0.09}_{-0.08}$	$1.28^{+0.06}_{-0.05}$	$48.7^{+0.9}_{-0.8}$	$4.3^{+0.8}_{-0.7}$	$1.1^{+0.4}_{-0.3}$	14.6	1.15(494)
20	81.13	$0.84^{+0.10}_{-0.10}$	$-0.04^{+0.06}_{-0.06}$	$6.98^{+0.23}_{-0.18}$	$0.25^{+0.02}_{-0.02}$	$27.12^{+0.08}_{-0.08}$	$4.00^{+0.10}_{-0.09}$	$1.34^{+0.08}_{-0.06}$	$49.4^{+0.9}_{-0.8}$	$5.3^{+0.8}_{-0.7}$	$1.3^{+0.4}_{-0.3}$	12.1	1.13(494)
21	88.86	$0.82^{+0.10}_{-0.10}$	$-0.05^{+0.06}_{-0.06}$	$6.93^{+0.34}_{-0.24}$	$0.18^{+0.01}_{-0.01}$	$27.34^{+0.12}_{-0.12}$	$4.00^{+0.15}_{-0.14}$	$1.32^{+0.11}_{-0.09}$	$48.6^{+1.0}_{-1.0}$	$4.9^{+1.2}_{-1.1}$	$1.2^{+0.6}_{-0.4}$	8.9	1.13(494)
22	105.04	$0.81^{+0.10}_{-0.10}$	$-0.05^{+0.07}_{-0.06}$	$7.03^{+0.61}_{-0.31}$	$0.06^{+0.01}_{-0.01}$	$27.68^{+0.15}_{-0.15}$	$3.71^{+0.19}_{-0.17}$	$1.34^{+0.16}_{-0.12}$	47^{+2}_{-1}	$4.6^{+1.8}_{-0.9}$	$1.4^{+1.2}_{-0.5}$	2.9	1.12(494)

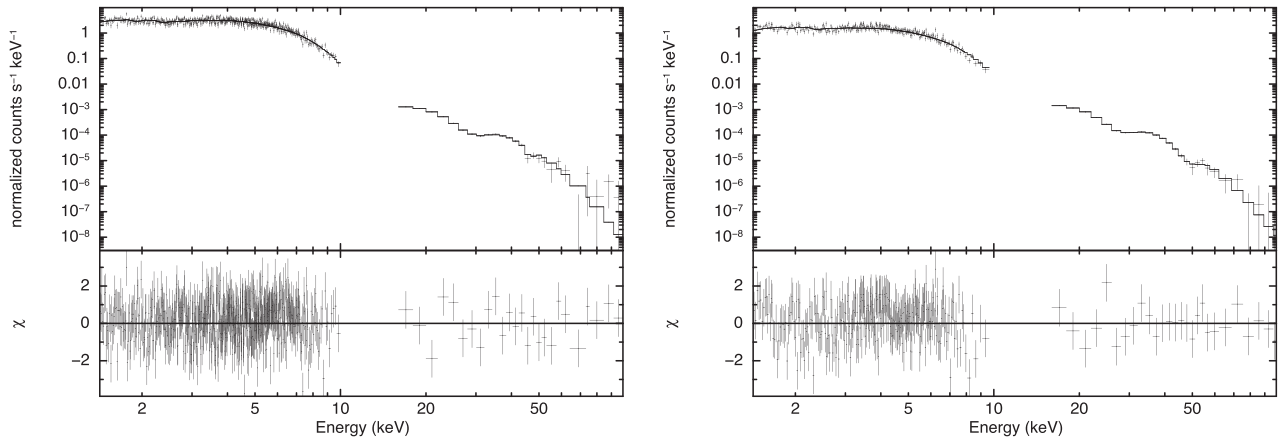


Figure 2. Data, best-fitting model and residuals for spectra 2 (left-hand panel) and 21 (right-hand panel).

parameters. Fig. 3 shows the confidence contour plots between the energy of the fundamental and the photon index, the cutoff energy and the width of the line, respectively, evaluated for the two representative spectra 2 and 21. The plots show that there is no significant correlation between $E_{\rm cyc}$ and the continuum parameters, and a weak correlation between $E_{\rm cyc}$ and the line width σ. The single-parameter 68 per cent error ranges evaluated from the fit procedure represent adequately the bidimensional confidence contours. Moreover, for each couple of parameters, the contour plots relevant to the two spectra are very well detached. We have also checked if the variability path we observe in the line energy is biased by the variation of $E_{\rm cut}$ measured along the outburst. Therefore, we have fitted the spectra fixing $E_{\rm cut}$ to the average of the values reported in Table 1, obtaining again a double track that overlaps with excellent agreement the one obtained when $E_{\rm cut}$ is left as a free parameter (Fig. 4, grey triangles). Finally, we note that cyclotron lines may

Downloaded from https://academic.oup.com/mnrasl/article-abstract/460/1/L99/2589767 by guest on 23 April 2020

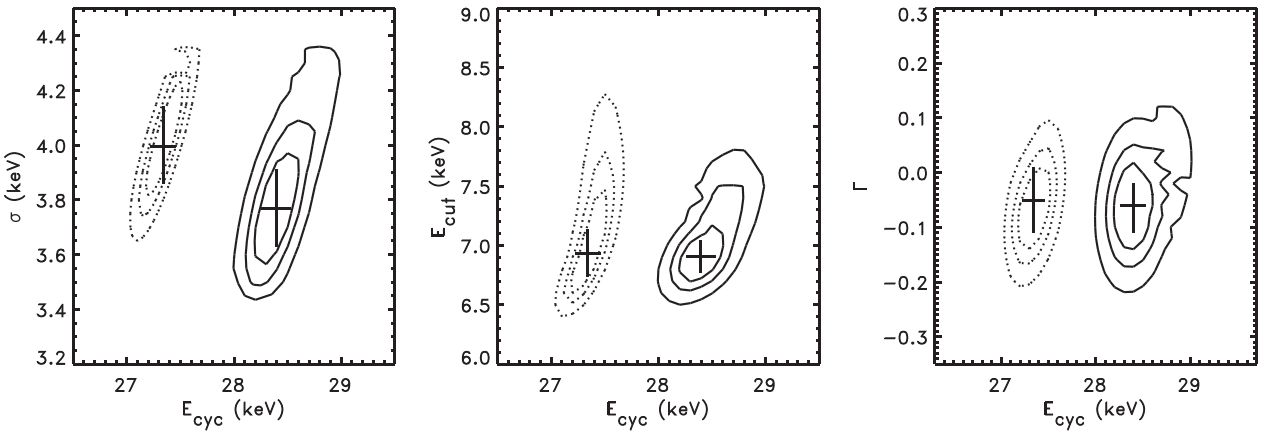


Figure 3. Confidence contour plots for three pairs of fit parameters, evaluated for spectra 2 (solid line) and 21 (dotted line). Contours are at 68, 90 and 99 per cent. The bars indicate the 68 per cent confidence error ranges reported in Table 1.

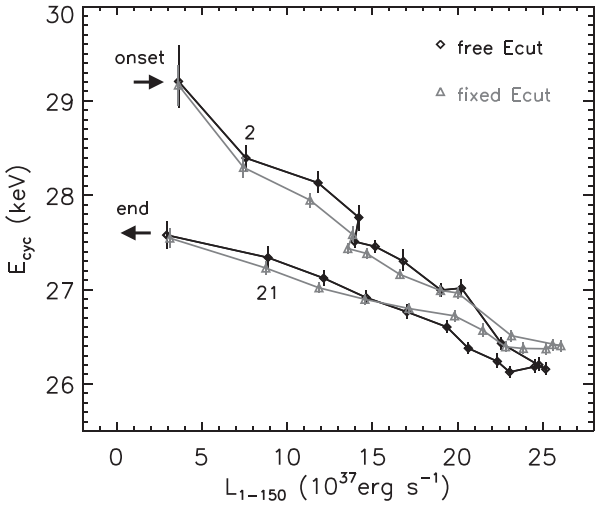


Figure 4. Position of the fundamental cyclotron line as a function of luminosity. The line connecting the points indicates their temporal sequence. The black diamonds are obtained fitting the spectra with E_{cut} as a free parameter. The grey triangles are obtained fixing E_{cut} to an average value of 6.65 keV.

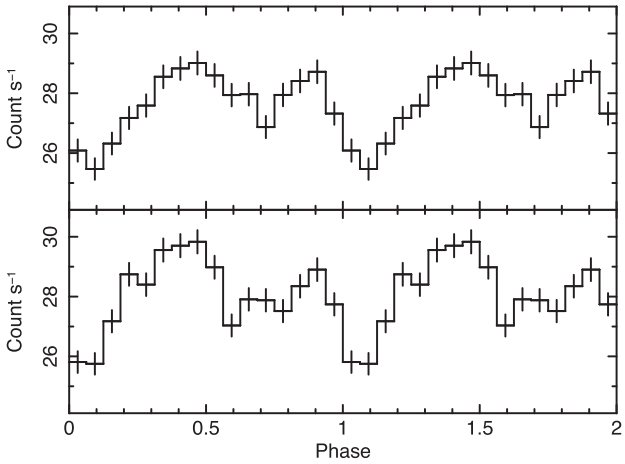


Figure 5. Pulse profiles obtained using the XRT data close to BAT intervals 2 (XRT ObsID 00031293007, 00031293008, 00031293009, top panel) and 21 (XRT ObsID 00081588002, 00081588003, bottom panel).

have complex profiles (Schönherr et al. 2007; Nishimura 2013), as also reported by some authors for V0332+53 (Pottschmidt et al. 2005; Nakajima, Mihara & Makishima 2010). The observational limits in our data do not allow us to assess if a change in the line profile could affect the determination of the centroid energy, although we argue that, if present, such a systematic would hardly produce systematically different line centroids at equal luminosities as shown in Fig. 4.

4 DISCUSSION

The anticorrelation between the fundamental CRSF energy and luminosity was already observed in the 2004/05 outburst (Tsygankov et al. 2010). However, in the 2015 outburst we find a remarkably significant difference in the path described by the cyclotron energy versus luminosity: while in the 2004/05 outburst the energy of the fundamental appears to follow the same path both during the rise and the decline, so that the intensity of the magnetic field is the same at the onset and at the end of the outburst, in 2015 the energy of the fundamental follows two distinct tracks, with a difference of ∼1.5 keV between the energy measured at the onset and at the end of the outburst. Lutovinov et al. (2015) have shown that the energy of the fundamental is variable with the pulse phase and that the variability pattern changes for different luminosity levels. They explain this behaviour with a change in the beam pattern along the line of sight and in the structure of the emission region. The interpulse variability pattern may affect the position of the CRSF fundamental in the phase-averaged spectra, and if the double track in Fig. 4 arises from different variability patterns in E_{cyc} at equal luminosity levels, we would expect a corresponding change in the pulse profiles. We have produced 0.3–10 keV pulse profiles using the XRT data collected along the outburst: the profile shows a substantial shape evolution, from a double peak profile at low luminosity to a single peak at high luminosity (see also Tsygankov et al. 2006). Fig. 5 shows that the profiles at similar luminosity levels close to the beginning and the end of the outburst have consistent shapes. Indeed, while both cyclotron line energy and pulse profile shape are known to change significantly with pulse phase and luminosity (Tsygankov et al. 2006; Lutovinov et al. 2015), a significant fraction of the energy flux is emitted in the soft band where, as we demonstrated, the pulse profile remains stable. Therefore, the comparison of the XRT profiles in the soft X-rays provides a hint against the hypothesis of a geometrical beam variation.

Downloaded from https://academic.oup.com/mnrasl/article-abstract/460/1/L99/2589767 by guest on 23 April 2020

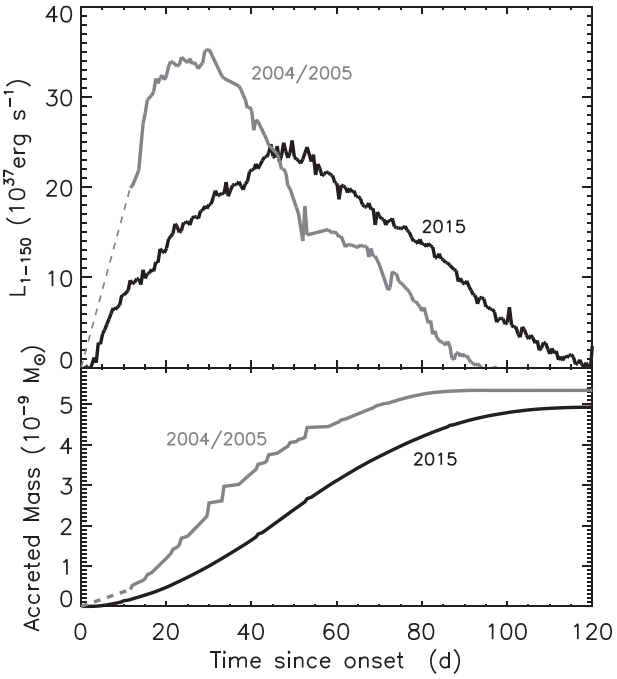


Figure 6. Top panel: light curve of the 2015 (black line) and of the 2004/05 (grey line) outbursts, reported to the same onset time. For the first 15 d of the 2004/05 outburst (not observed by BAT), we assume a linear rise (dashed grey line) as suggested by the RXTE All-Sky Monitor light curve. Bottom panel: total accreted mass as a function of time, according to $L_{1-150} = \eta \dot{M} c^2$, where we adopt a mass-energy conversion factor $\eta = 0.15$, as commonly assumed for an NS.

If, on the other hand, the line-forming region is the same at equal luminosities, the observed difference in the cyclotron energy corresponds to a difference in the magnetic field of $\sim 1.7 \times 10^{11}$ G (assuming $z = 0.3$ at the surface of an NS with a mass of 1.4 $M_\odot$ and a radius of 10 km).

An intriguing question is why the field drop has not been observed also in the 2004/05 outburst. Fig. 6, that compares the light curves of the two outbursts (top panel) and the cumulative accreted mass (bottom panel), shows a substantial difference: although the total mass accreted at the end of the two outbursts is similar, during the 2004/05 outburst a higher luminosity (1.5 times that of 2015) is reached earlier. Therefore, we argue that the splitting in two branches of the $E_{\rm cyc}$ versus L_{1-150} depends on how the mass accretes along the outburst, and not simply on the total accreted mass, in agreement with previous suggestions that the decay of the magnetic field is not directly proportional to the total accreted mass (Wijers 1997).

Among the several mechanism that can induce a decay of the magnetic field through accretion (see e.g. Ruderman 1991; Cumming, Arras & Zweibel 2004; Lovelace, Romanova & Bisnovatyi-Kogan 2005) the one that seems to accord better with the observations is diamagnetic screening (Chouduri & Konar 2002). In this hypothesis, the accreting plasma builds up to form a magnetically confined mound, where the gas pressure balances the magnetic stresses. This would produce, as an overall effect, a distortion of the field lines (Brown & Bildstein 1998) observed as a decrease of the field component along the accretion column. However, for higher peak luminosities, the magnetic cap surface is larger and it is conceivable that the field at its border is weaker, preventing the gas confinement. The fast rise time observed in the 2004/05 outburst could lead to this configuration at the very beginning of the outburst, hampering the formation of the mound. Alternatively, the mound may have formed at an early stage of the outburst, reaching in a short time the maximum size for a stable structure. After that, an equilibrium was reached where the plasma settling on the mound was balanced by the matter leaking out from the mound. In this hypothesis, we expect that for most of the outburst evolution the tracks do not diverge. This hypothesis is suggested by the first two points of the outburst rise in fig. 3 in Tsygankov et al. (2010), that show $E_{\rm cyc}$ values significantly higher than the values at equal luminosity during the decline. However, the lack of coverage in the first 10 days of the outburst prevents a firm conclusion on this point.

ACKNOWLEDGEMENTS

This work has been supported by ASI grant I/004/11/1.

REFERENCES

Barthelmy S. et al., 2005, Space. Sci. Rev., 120, 143
Basko M. M., Sunyaev R. A., 1976, MNRAS, 175, 395
Becker P. A. et al., 2012, A&A, 544, 123
Brown E. F., Bildsten L., 1998, ApJ, 496, 915
Burnard D. J., Arons J., Klein R. I., 1991, ApJ, 376, 575
Burrows D. N. et al., 2005, Space. Sci. Rev., 120, 165
Choudhuri A. R., Konar S., 2002, MNRAS, 332, 933
Cumming A., Arras P., Zweibel E., 2004, ApJ, 609, 999
Gehrels N. et al., 2004, ApJ, 611, 1005
Hill J. et al., 2004, SPIE, 5165, 217
Lovelace R. V. E., Romanova M. M., Bisnovatyi-Kogan G. S., 2005, ApJ, 625, 957
Lutovinov A. A., Tsygankov S. S., Suleimanov V. F., Mushtukov A. A., Doroshenko V., Nagirner D. I., Poutanen J., 2015, MNRAS, 448, 2175
Makishima K et al., 1990, ApJ, 365, L59
Mihara T., Makishima K., Nagase F., 1995, BAAS, 27, 1434
Mowlavi N. et al., 2006, A&A, 451, 187
Nakajima M., Mihara T., Makishima K., 2010, ApJ, 710, 1755
Negueruela I., Roche P., Fabregat J., Coe M. J., 1999, MNRAS, 307, 695
Nishimura O., 2013, PASJ, 65, 84
Pottschmidt K. et al., 2005, ApJ, 634, L97
Revnivtsev M., Mereghetti S., 2015, Space Sci. Rev., 191, 293
Ruderman M., 1991, ApJ, 366, 261
Schönherr G., Wilms J., Kretschmar P., Kreykenbohm I., Santangelo A., Rothschild R. E., Coburn W., Staubert R., 2007, A&A, 472, 353
Segreto A., Cusumano G., Ferrigno C., La Parola V., Mangano V., Mineo T., Romano P., 2010, A&A, 510, 47
Stella L., White N. E., Davelaar J., Parmar A. N., Blissett R. J., van der Klis M., 1985, ApJ, 288, L45
Tsygankov S. S., Lutovinov A. A., Churazov E. M., Sunyaev R. A., 2006, MNRAS, 371, 19
Tsygankov S. S., Lutovinov A. A., Serber A. V., 2010, MNRAS, 401, 1628
Wijers R. A. M. J., 1997, MNRAS, 287, 607

This paper has been typeset from a TEX/LATEX file prepared by the author.

Downloaded from https://academic.oup.com/mnrasl/article-abstract/460/1/L99/2589767 by guest on 23 April 2020